Geophysical Research Letters

RESEARCH LETTER
10.1002/2018GL077548

Key Points:
- Stress variability in fractured geological media is simulated using a geomechanical model and characterized using a tensor-based formalism
- Local stress perturbation has a positive, linear correlation with local fracture intensity in fractured rocks
- Strong stress dispersion occurs in a well-connected fracture system under a critically stressed state for frictional sliding

Supporting Information:
- Supporting Information S1

Correspondence to:
Q. Lei and K. Gao,
q.lei12@imperial.ac.uk;
k.gao@mail.utoronto.ca

Citation:
Lei, Q., & Gao, K. (2018). Correlation between fracture network properties and stress variability in geological media. *Geophysical Research Letters*, *45*. https://doi.org/10.1002/2018GL077548

Received 3 OCT 2017
Accepted 27 MAR 2018
Accepted article online 31 MAR 2018

Correlation Between Fracture Network Properties and Stress Variability in Geological Media

Qinghua Lei[1] and **Ke Gao**[2]

[1]Department of Earth Science and Engineering, Imperial College London, London, UK, [2]Department of Civil Engineering, University of Toronto, Toronto, Ontario, Canada

Abstract We quantitatively investigate the stress variability in fractured geological media under tectonic stresses. The fracture systems studied include synthetic fracture networks following power law length scaling and natural fracture patterns based on outcrop mapping. The stress field is derived from a finite-discrete element model, and its variability is analyzed using a set of mathematical formulations that honor the tensorial nature of stress data. We show that local stress perturbation, quantified by the Euclidean distance of a local stress tensor to the mean stress tensor, has a positive, linear correlation with local fracture intensity, defined as the total fracture length per unit area within a local sampling window. We also evaluate the stress dispersion of the entire stress field using the effective variance, that is, a scalar-valued measure of the overall stress variability. The results show that a well-connected fracture system under a critically stressed state exhibits strong local and global stress variabilities.

Plain Language Summary Knowledge of the stress state in the Earth's crust is of great importance for many scientific and engineering problems, such as earthquake prediction, petroleum recovery, groundwater management, underground excavation, and deep geological disposal of radioactive/toxic waste. However, it is very challenging to fully understand the stress state, because it is highly variable in the subsurface. One of the key factors is the presence and complexity of natural fractures in rock. Then, a fundamental question is raised: is the stress field correlated with these fractures? How? To answer this question, we build numerical models to calculate the stress state in geological media embedded with realistic fracture networks. We utilize a new mathematical approach to process the simulation data. We report that the local stress fluctuation is strongly related to the local fracture distribution, and the overall stress variability is greatly controlled by the fracture network connectivity.

1. Introduction

Characterization of the stress state in the Earth's crust is essential for earthquake prediction and subsurface engineering (McGarr & Gay, 1978; Zoback, 2007). Over the past half-century, great efforts have been devoted to the measurement of in situ stresses (Amadei & Stephansson, 1997; Bell & Gough, 1979; Haimson, 1975; Hast, 1969; Kropotkin, 1972; Zoback et al., 1989). The state of stress in the crust is mainly governed by tectonic stresses and local perturbations (Hudson & Cooling, 1988; Zoback et al., 1989). Tectonic stresses related to plate-driving forces are typically uniform over the lithospheric scale (Zoback et al., 1989), while local perturbations induced by topography, discontinuity, material inhomogeneity, and anisotropy as well as engineering processes have much smaller wavelengths (Zoback, 1992). The superimposition of the two categories of forces often leads to locally varying stress patterns (Hudson & Cooling, 1988; Shamir & Zoback, 1992; Yale, 2003). Extensive field data have suggested that fractures, such as faults and joints, play an important role in perturbing the regionally uniform tectonic stress field (Barton & Zoback, 1994; Bruno & Winterstein, 1992; Day-Lewis et al., 2010; Hickman & Zoback, 2004; Lin et al., 2007, 2010; Martin & Chandler, 1993; Mcnamara et al., 2015; Rajabi et al., 2017; Sahara et al., 2014; Schoenball & Davatzes, 2017; Shamir & Zoback, 1992; Stephansson et al., 1991; Townend & Zoback, 2004; Valley, 2007; Yale, 2003). In these previous studies, such perturbation effects were characterized using customary scalar/vector approaches, which separately analyze the principal stress magnitude and orientation. However, we argue that stress is a tensor in nature and its perturbation needs to be quantified in an integrated formalism incorporating both orientation and magnitude alterations. Thus, a key objective of this paper is to propose a framework, which is faithful to the tensorial nature of stress, to quantify stress variability in fractured geological media. In this context, the underlying relationships among fracture geometry, tectonic stresses, frictional sliding, and stress variability are explored based on the state-of-the-art numerical simulation.

In this study, we focus on the two-dimensional (2-D) scenario, which may be relevant to geological formations whose longitudinal characteristic scale is much larger than transversal ones. We analyze both the synthetic fracture networks following power law length scaling and natural fracture networks mapped from a real outcrop. We assume that fracture pattern is the result of paleo-stress evolution and has little correlation with the contemporary tectonic stress field, which is a scenario often observed in nature (Amadei & Stephansson, 1997; Zoback, 2007). We also hypothesize that stress perturbation in the fractured rock develops entirely based on contemporary tectonic stresses, whereas the complex residual stress effect is not considered. The paper focuses on a fixed scale of interest, whereas the analysis of scale effect is beyond the current scope.

2. Methodology

2.1. Fracture Network Generation and Characterization

Natural fracture systems often exhibit a broad range of fracture lengths that can be described by a power law model (Bonnet et al., 2001; Bour & Davy, 1999; Lei & Wang, 2016):

$$n(l,L) = \alpha L^D l^{-a}, \qquad \text{for } l \in [l_{\min}, l_{\max}], \tag{1}$$

where $n(l, L)dl$ is the number of fractures with sizes l belonging to the interval $[l, l + dl]$ ($dl \ll l$) in an elementary volume of characteristic size L, D is the fractal dimension, a is the power law length exponent, and α is the density term. The only intrinsic characteristic length scales in this model are the smallest and largest fracture lengths, that is, $l_{\min}$ and $l_{\max}$, respectively. In numerical simulations, L is the scale of the modeling domain, which usually meets $l_{\min} \ll L \ll l_{\max}$. The exponents D and a quantify different scaling aspects of fracture networks: the fracture density (related to D) and the length distribution (related to a). Extensive outcrop data suggest that generally D varies between 1.5 and 2.0, and a falls between 1.3 and 3.5 (Bonnet et al., 2001).

Fracture intensity is defined as the total length of fractures per unit area. The mean fracture intensity $\bar{\gamma}$ of a fracture network within a squared domain of size L is calculated as

$$\bar{\gamma} = \frac{1}{L^2} \int_{A_L} n(l,L) l' dl, \tag{2}$$

where l' denotes the fracture length included in the domain of an area $A_L = L^2$. The local fracture intensity γ is measured using a circular window approach (Mauldon et al., 2001):

$$\gamma = \frac{1}{\pi r^2} \int_{A_r} n(l,L) l' dl, \tag{3}$$

where l' denotes the fracture length included in a circular window of an area $A_L = \pi r^2$ and the radius r is substituted using $1/\bar{\gamma}$, which approximates to half of the average spacing (or block size) of a fracture system (Dershowitz & Herda, 1992). The variance of local fracture intensity σ^2 thus indicates the geometric heterogeneity of the fracture network.

The geometric connectivity of a fracture network may be assessed using the percolation parameter:

$$p(l,L) = \int_{A_L} \frac{n(l,L) l'^2}{L^2} dl, \tag{4}$$

which is applicable for nonfractal fracture networks with $D = 2.0$ (Bour & Davy, 1997), and fractal fracture networks satisfying $a \leq D + 1$ (Darcel, Bour, Davy, & de Dreuzy, 2003; Davy et al., 2010). The higher the p is, the more connected the system is. The network is statistically connected if p is greater than the percolation threshold p_c, which may have a scale-independent value of ~5.8 (Bour & Davy, 1997). Uncertainties may exist in this p_c value when being applied to fracture patterns involving distinguishable orientation sets (Robinson, 1983, 1984) and fractal density distributions (Darcel, Bour, Davy, & de Dreuzy, 2003).

In this study, we generate a series of 2-D synthetic and natural fracture networks in a squared domain of size $L = 10$ m (Figure 1). In the synthetic networks, the location and orientation of fractures are assumed purely random, that is, nominally homogeneous (i.e., $D = 2.0$) and isotropic. The fracture lengths follow the power law scaling, with the bounds given by $l_{\min} = L/50 = 0.2$ m and $l_{\max} = 50\ L = 500$ m. We explore five different length exponent cases, that is, a = 1.5, 2.0, 2.5, 3.0, and 3.5, and two different mean fracture intensity

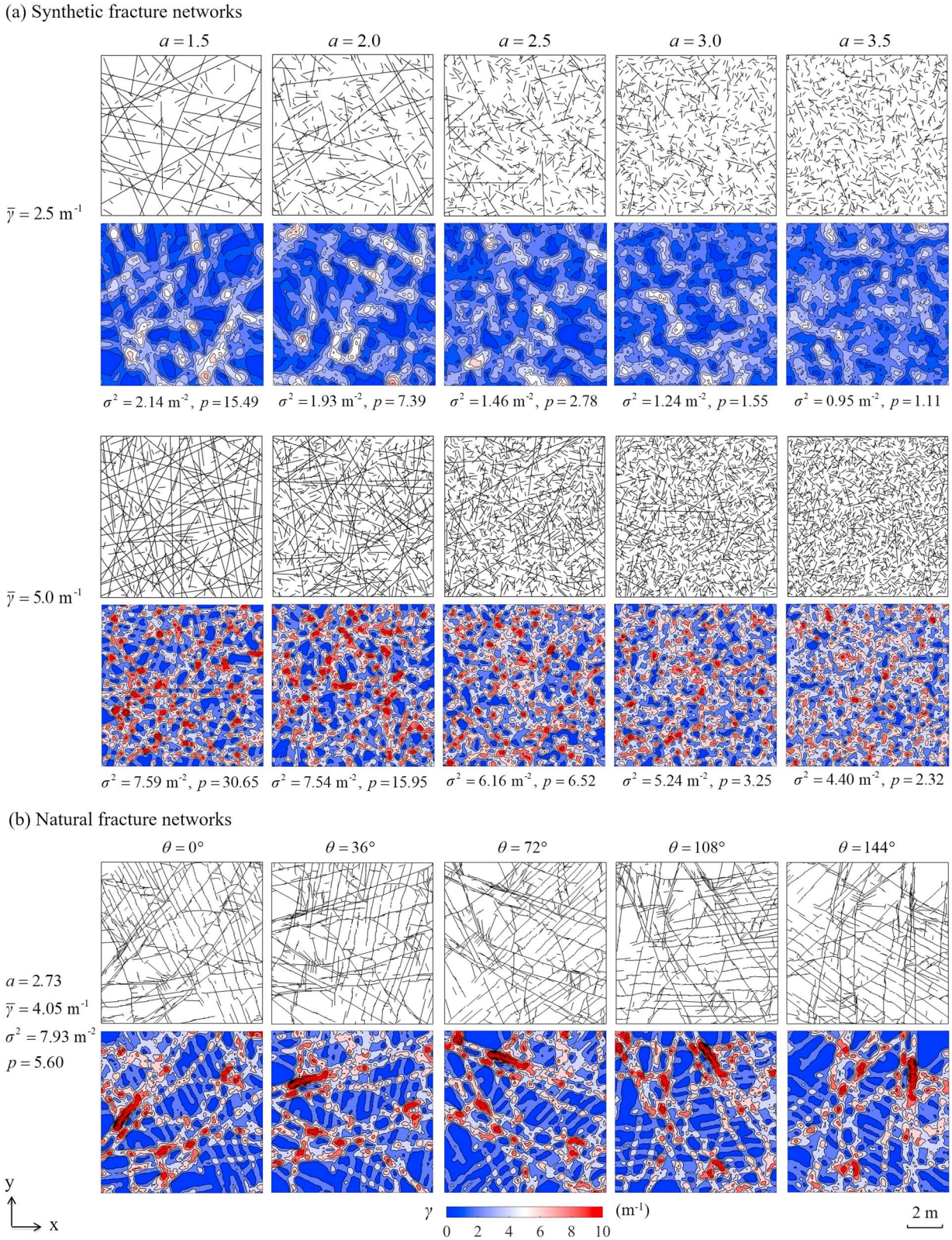

Figure 1. (a) The geometry and local fracture intensity γ of synthetic fracture networks (domain size L = 10 m) associated with various power law length exponent a and mean fracture intensity $\bar{\gamma}$. (b) The geometry and local fracture intensity γ of natural fracture networks (domain size L = 10 m) extracted from the outcrop pattern at the Hornelen Basin (Odling, 1997) using a sampling window rotated at different angles θ. The variance of local fracture intensity σ^2 and the percolation parameter p are shown for each network.

scenarios, that is, $\overline{\gamma}$ = 2.5 and 5.0 m^{-1}. For each combination of a and $\overline{\gamma}$, 10 realizations are generated, with their σ^2 and p values also derived. As shown in Figure 1a, with the increase of a, the system becomes more dominated by small fractures, and vice versa. It can be seen that local fracture intensity exhibits high values in the vicinity of fractures, especially at fracture intersections. An increased a leads to a reduction in both the geometric connectivity (decreased p) and heterogeneity (decreased σ^2). It is worth mentioning that the stress shadow effect on fracture organization (Ackermann & Schlische, 1997; Darcel, Bour, & Davy, 2003; Davy et al., 2010; Segall & Pollard, 1983) is not considered in the synthetic fracture network generation. We therefore also extract natural fracture networks from a real outcrop exposed at the Hornelen Basin (Odling, 1997) using a sampling window rotated at different angles θ = 0°, 36°, 72°, 108°, and 144° (Figures 1b and S1). The a and D values of this natural fracture system are 2.73 and 1.80, respectively (Bour et al., 2002), while $\overline{\gamma}$, σ^2, and p are calculated to be 4.05 m^{-1}, 7.93 m^{-2}, and 5.60, respectively. The large σ^2 value is attributed to the spatial clustering feature ($D < 2.0$).

2.2. Numerical Method and Geomechanical Model

The plane-strain deformation of a 2-D fractured rock in response to tectonic stresses is modeled using the hybrid finite-discrete element method (FEMDEM) (Munjiza, 2004), which can realistically simulate the stress in intact rocks, interaction between matrix blocks, deformation of natural fractures, and propagation of new cracks (Lei et al., 2015, 2017). More details of the FEMDEM approach are given in the supporting information, including the governing equation (Text S1), space discretization (Figure S2), and validation for stress computation (Figures S3 and S4).

The material properties of the fractured rock are assumed as follows (Lama & Vutukuri, 1978; Zoback, 2007): the bulk density is 2,700 kg/m^3, the Young's modulus is 50.0 GPa, the Poisson's ratio is 0.25, the internal friction coefficient is 1.0, the tensile strength is 20.0 MPa, the cohesive strength is 40.0 MPa, and the mode I and II energy release rates are 158.4 and 198.0 J/m^2, respectively. The shear strength of fractures obeys the Coulomb criterion such that frictional sliding occurs if the shear stress exceeds the product of the effective normal stress and the friction coefficient μ. Three typical μ values are explored, that is, 0.6, 0.85 and 1.0 (Byerlee, 1978; Zoback, 2007). The problem domain containing distributed fractures is discretized using an unstructured mesh with an average element size of 0.05 m. The penalty term and damping coefficient are chosen to be 500 GPa and 2.0×10^5 kg/ms, respectively. Effective tectonic principal stresses are loaded orthogonally to the model, and we consider three different stress scenarios: (i) S_{xx}^{∞} = 5.0 MPa, S_{yy}^{∞} = 5.0 MPa; (ii) S_{xx}^{∞} = 10.0 MPa, S_{yy}^{∞} = 5.0 MPa; and (iii) S_{xx}^{∞} = 15.0 MPa, S_{yy}^{∞} = 5.0 MPa, such that the tectonic stress ratio $S_{xx}^{\infty}/S_{yy}^{\infty}$ = 1.0, 2.0, and 3.0, respectively.

2.3. Tensor-Based Quantification of Stress Variability

We obtain the stress field from the FEMDEM simulation in which all components of the second-rank Cauchy stress tensor at each element node are determined. We analyze the stress data using the recently developed tensor-based mathematical formulations (Gao, 2017; Gao & Harrison, 2016, 2018), which overcome the drawbacks of conventional decoupled analysis of stress magnitude and orientation information (further discussions are in Text S2 and Figure S5).

In a 2-D stress tensor field $\mathbf{S}$, which consists of n stress measurements, the ith stress tensor $\mathbf{S}_i$ is written as

$$\mathbf{S}_i = \begin{bmatrix} S_{xx,i} & S_{xy,i} \\ \text{symmetric} & S_{yy,i} \end{bmatrix}. \tag{5}$$

The mean of the entire stress field is calculated as (Gao & Harrison, 2016)

$$\overline{\mathbf{S}} = \frac{1}{n}\sum_{i=1}^{n}\mathbf{S}_i = \frac{1}{n}\begin{bmatrix} \sum_{i=1}^{n} S_{xx,i} & \sum_{i=1}^{n} S_{xy,i} \\ \text{symmetric} & \sum_{i=1}^{n} S_{yy,i} \end{bmatrix}, \tag{6}$$

which was derived by introducing the Euclidean distance between stress tensors and using a fundamental definition of mean in statistics—Fréchet mean function (Pennec, 2009). For two stress tensors $\mathbf{S}_i$ and $\mathbf{S}_j$, their Euclidean distance is given by

$$d(\mathbf{S}_i, \mathbf{S}_j) = \|\mathbf{S}_i - \mathbf{S}_j\|_F, \quad 1 \le i \le n \text{ and } 1 \le j \le n, \tag{7}$$

where $\|\cdot\|$ denotes the Frobenius norm (also known as the Euclidean norm or Hilbert-Schmidt norm; Gentle, 2007). Thus, the mean stress is the stress tensor $\mathbf{Y}$ that minimizes the expectation of the squared Euclidean distance between each stress tensor $\mathbf{S}_i$ and $\mathbf{Y}$, that is,

$$\overline{\mathbf{S}} = \arg \min_{\mathbf{Y}} \left(\frac{1}{n} \sum_{i=1}^{n} \|\mathbf{Y} - \mathbf{S}_i\|_F^2 \right), \tag{8}$$

which leads to equation (6).

It has been proven that the mean stress tensor in a fractured rock equals to the far-field stress tensor, that is, the tectonic stress tensor (Gao et al., 2017), which has also been verified in this work (Figure S16). Thus, we can use the Euclidean distance between a local stress tensor $\mathbf{S}_i$ and the mean stress tensor $\overline{\mathbf{S}}$:

$$d(\mathbf{S}_i, \overline{\mathbf{S}}) = \|\mathbf{S}_i - \overline{\mathbf{S}}\|_F, \tag{9}$$

which measures how far away a local stress tensor is from the mean stress, as an indicator of local stress perturbation to the tectonic stress environment. In a purely uniform stress field, $d(\mathbf{S}, \overline{\mathbf{S}})$ is zero throughout, while in a highly variable stress field, $d(\mathbf{S}, \overline{\mathbf{S}})$ could change significantly from point to point.

The variability of stress tensor data can be adequately represented by the variability of their distinct tensor components in a multivariate statistics manner (Gao & Harrison, 2018). The overall dispersion of a stress field can thus be described by its effective variance—a widely used concept in the field of multivariate statistics for group variability comparison (Peña & Rodríguez, 2003). For a stress tensor $\mathbf{S}_i$, its distinct components form a stress vector $\mathbf{s}_i$ as

$$\mathbf{s}_i = \text{vech}(\mathbf{S}_i) = [\, S_{xx,i} \quad S_{yx,i} \quad S_{yy,i} \,]^T = [\, S_{xx,i} \quad S_{xy,i} \quad S_{yy,i} \,]^T, \tag{10}$$

where vech(·) is the half-vectorization function that stacks only the lower triangular (i.e., on and below the diagonal) columns of a tensor into a column vector containing only the distinct components. The effective variance is then calculated as (Gao, 2017)

$$V_e(\mathbf{S}) = \sqrt[\frac{1}{2}m(m+1)]{\det(\mathbf{\Omega})}, \tag{11}$$

where m is the dimension of the stress tensor ($m = 2$ here) and $\mathbf{\Omega}$ is the covariance matrix of the stress vector field $\mathbf{s}$ (Gao & Harrison, 2017):

$$\Omega = \text{cov}(\mathbf{s}, \mathbf{s}) = \sum_{i=1}^{n} \left[(\mathbf{s}_i - \overline{\mathbf{s}}) \cdot (\mathbf{s}_i - \overline{\mathbf{s}})^T \right], \tag{12}$$

where $\overline{\mathbf{s}}$ is the mean stress vector:

$$\overline{\mathbf{s}} = \frac{1}{n} \sum_{i=1}^{n} \mathbf{s}_i. \tag{13}$$

The effective variance gives a scalar-valued measure of how spread out a stress tensor group is with respect to their mean, and it has the same unit as the variance of stress components, that is, square of the unit of stress. We use the effective variance $V_e(\mathbf{S})$ to characterize the bulk stress variability in fractured rocks. The larger the $V_e(\mathbf{S})$ is, the more dispersed the stress field is. It is worth clarifying that $d(\mathbf{S}, \overline{\mathbf{S}})$ measures the variation of local stress tensors, whereas $V_e(\mathbf{S})$ indicates the dispersion of the entire stress field.

3. Results

Figures 2 and 3 show the distributions of local stress perturbation and shear displacement, respectively, in the fractured rocks associated with $\mu = 0.6$ under different tectonic stress conditions (the cases of $\mu = 0.85$ and 1.0 are shown in Figures S6–S9). The stress and displacement patterns are quite uniform under the isotropic tectonic stress condition, whereas stronger fluctuations emerge in the anisotropic stress cases. As $S_{xx}^{\infty}/S_{yy}^{\infty}$ increases, significant shear displacement is accommodated along large fractures that are preferentially oriented for frictional sliding, while localized stress perturbation is manifest in the vicinity of the tips/intersections of these fractures, where intense mechanical interaction and brittle failure can occur. In

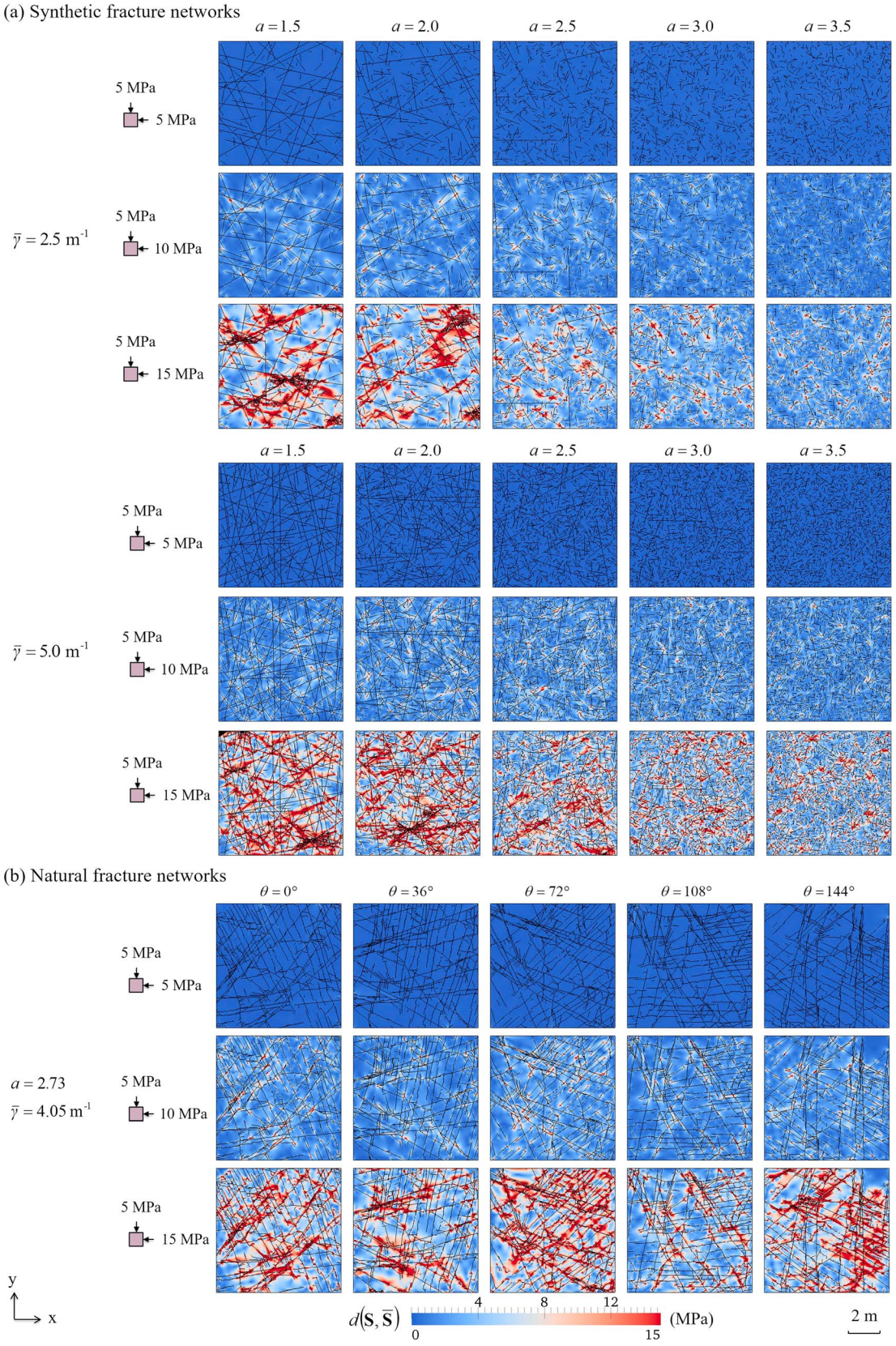

Figure 2. Distribution of local stress perturbation $d(\mathbf{S}, \bar{\mathbf{S}})$ in the synthetic and natural fracture networks associated with a friction coefficient of 0.6 under different tectonic stress conditions.

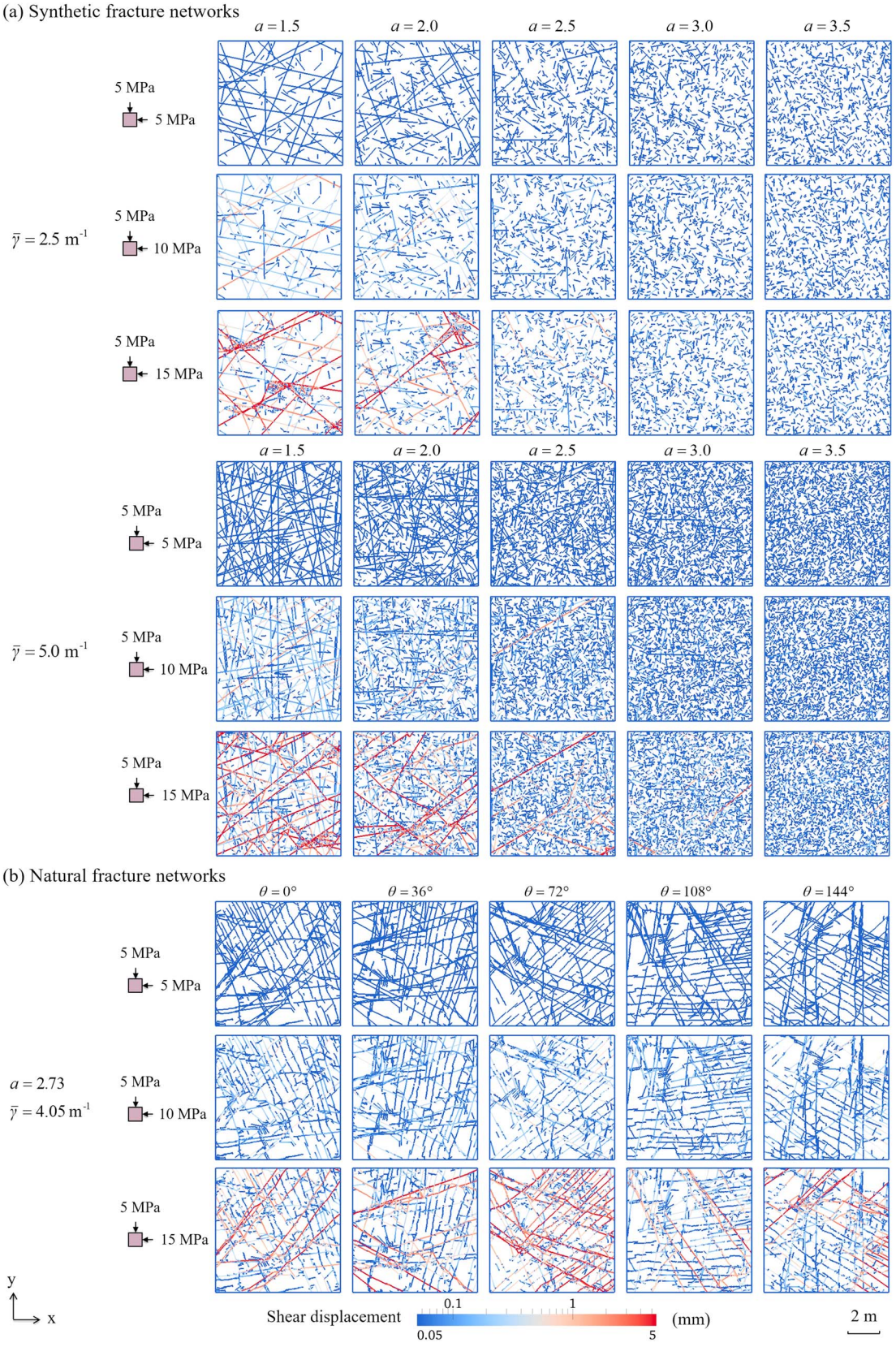

Figure 3. Distribution of shear displacement in the synthetic and natural fracture networks associated with a friction coefficient of 0.6 under different tectonic stress conditions.

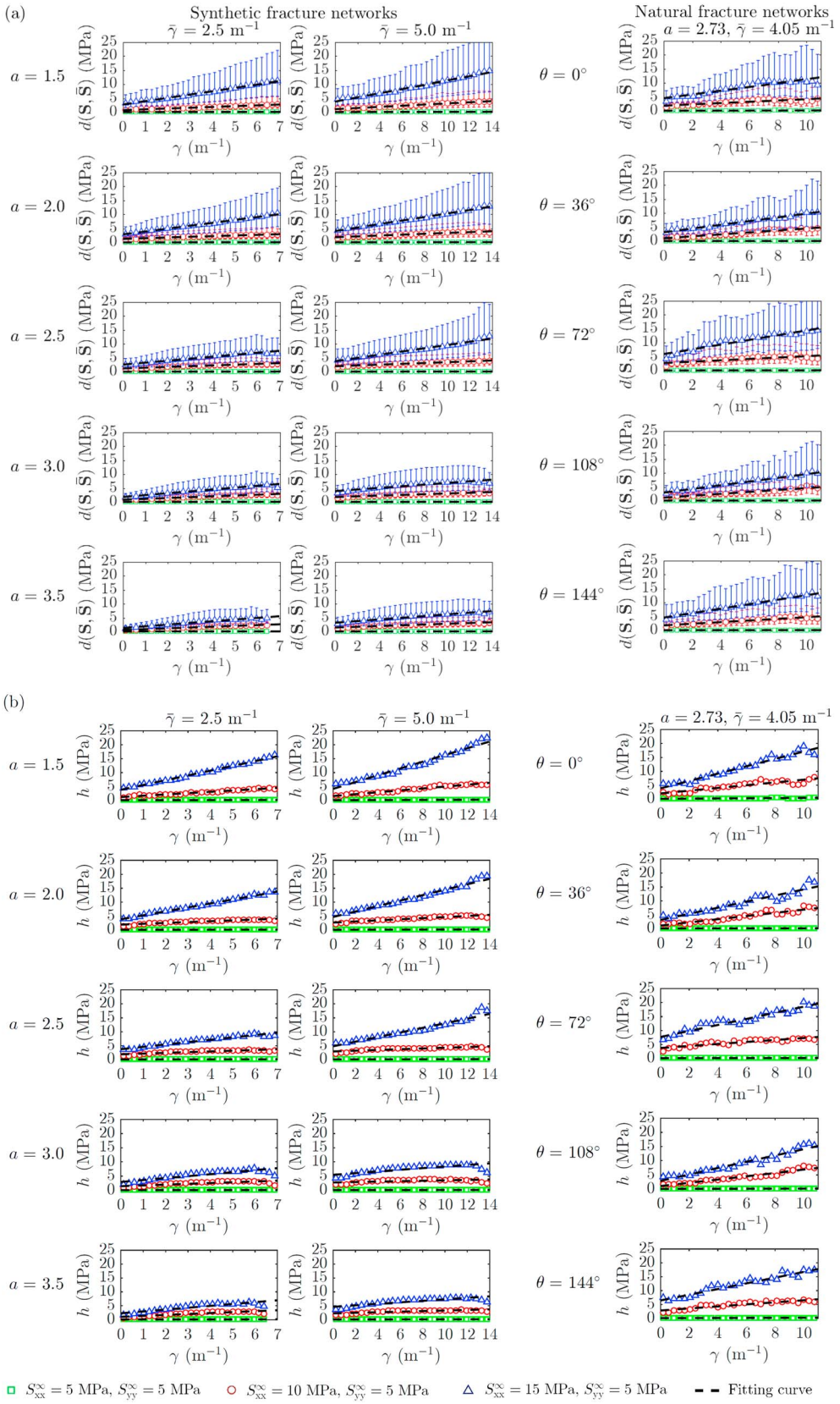

Figure 4. Variation of (a) local stress perturbation $d(\mathbf{S}, \bar{\mathbf{S}})$ and (b) its scatter h with local fracture intensity γ in the synthetic and natural fracture networks associated with a friction coefficient $\mu = 0.6$ under different tectonic stress conditions.

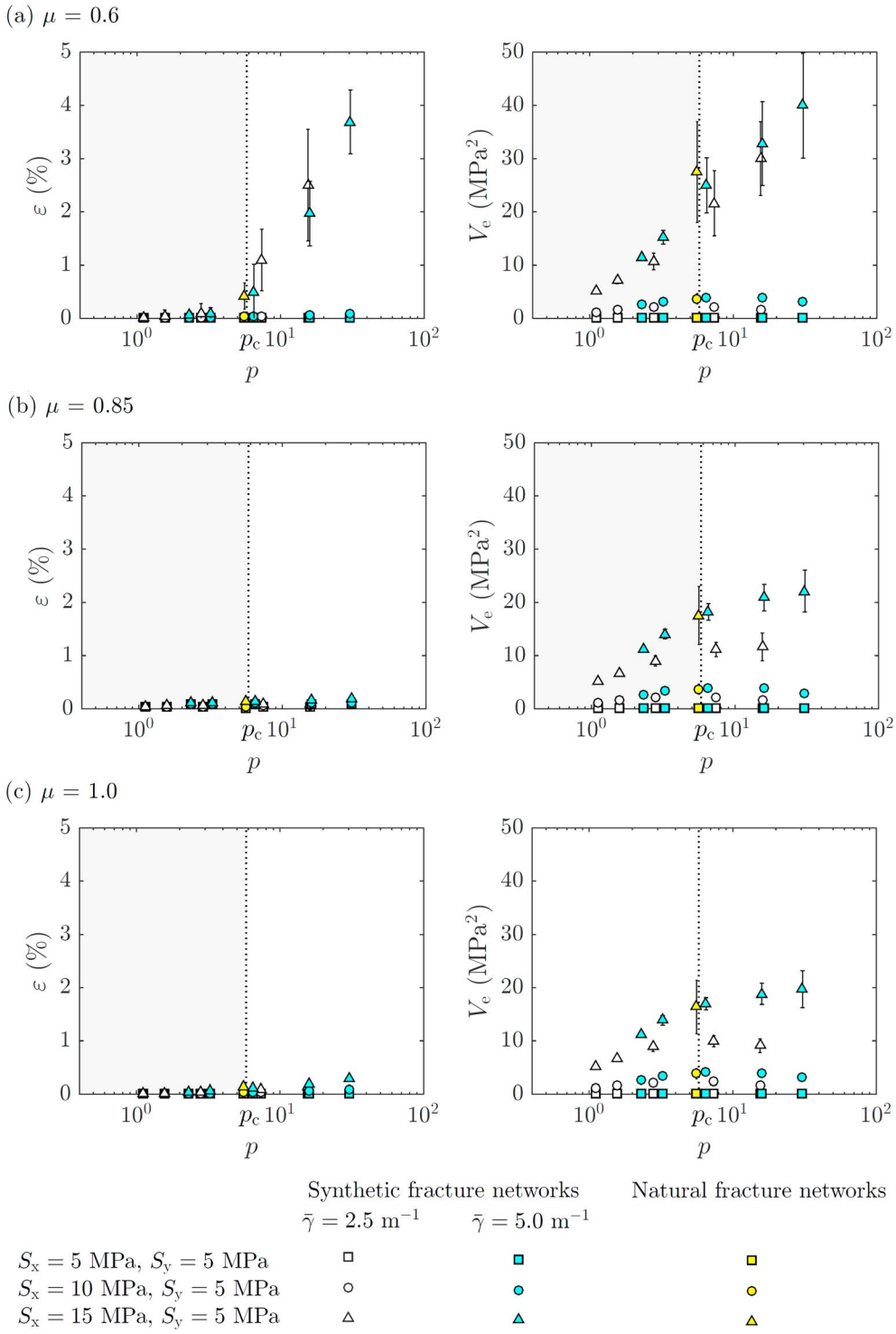

Figure 5. (left column) Variation of the total strain ε of frictional sliding and (right column) the effective variance $V_e(\mathbf{S})$ of the stress field as a function of the percolation parameter p of the fracture networks associated with different values of friction coefficient μ. The dotted line corresponds to the percolation threshold $p_c \approx 5.8$, across which the fracture system transits from disconnected to connected states. For the synthetic fracture networks, each data point represents the mean value of 10 realizations having the same a and $\bar{\gamma}$ values, and the error bar indicates the corresponding ±1 standard deviation. For the natural fracture networks, the marker and error bar respectively give the mean and ± 1 standard deviation of the results of the five extracted patterns.

the synthetic fracture networks, local stress perturbation and shear displacement are both enhanced as $\bar{\gamma}$ increases or a decreases (Figures 2a and 3a). In the natural fracture networks, the perturbation field varies with θ because of the anisotropic geometry of the fracture system, such that significant perturbation occurs when major sets of fractures are promoted for shearing, for example, when $\theta = 72°$ and $S_{xx}^{\infty}/S_{yy}^{\infty} = 3.0$ (Figures 2b and 3b). Furthermore, an increased μ tends to suppress frictional sliding and stress perturbation in both the synthetic and natural fracture networks (Figures S6–S9).

We analyze the relationship between local fracture intensity γ and local stress perturbation $d(\mathbf{S}, \bar{\mathbf{S}})$, which seems to fit to a positive, linear trend (Figures 4a, S10a, and S11a). Note that the geometric mean and standard deviation of each bin data of $d(\mathbf{S}, \bar{\mathbf{S}})$ are used due to their lognormal-like distribution (Figures S12–S14). Such a linear correlation tends to hold for different fracture networks, different friction coefficients, and different tectonic stress conditions. It is also noticed that the scatter h of $d(\mathbf{S}, \bar{\mathbf{S}})$ in each bin (i.e., the total length of the upper and lower error bars in Figures 4a, S10a, and S11a) also varies linearly with γ (Figures 4b, S10b, and S11b), further confirming the presence of a systematic correlation between fracture distribution and stress perturbation. The coefficients of the observed linear correlations are calculated in Text S3 and Figure S15, which show strong dependency on the tectonic stress condition.

We further study the relationship between the bulk strain/stress characteristics and the geometric connectivity of fracture networks (Figure 5). We calculate the total strain ε of frictional sliding as the sum of the geometric moments (i.e., product of the average shear displacement and fracture length) of all fractures divided by the area of the domain (Marrett & Allmendinger, 1991). As shown in Figure 5 (left panel), ε is very small if the fracture network is disconnected ($p < p_c$), due to the dominant matrix resistance against fractures for shearing. However, as the fracture network becomes connected ($p > p_c$), an abruptly increased strain is accommodated in the system, especially when $S_{xx}^{\infty}/S_{yy}^{\infty} = 3.0$ and $\mu = 0.6$. Such a transitional phenomenon is significantly attenuated in the cases of smaller $S_{xx}^{\infty}/S_{yy}^{\infty}$ and larger μ values. The overall stress variability in each fractured rock is characterized using the effective variance $V_e(\mathbf{S})$ of the entire stress tensor field. As can be seen in Figure 5 (right panel), the system exhibits much larger $V_e(\mathbf{S})$ when $S_{xx}^{\infty}/S_{yy}^{\infty} = 3.0$ as a result of intensive mechanical interactions driven by high differential stresses. Furthermore, as the system transits from disconnected to connected states (i.e., as p approaches and then exceeds p_c), $V_e(\mathbf{S})$ increases substantially, especially when $S_{xx}^{\infty}/S_{yy}^{\infty} = 3.0$. In the disconnected regime ($p < p_c$), $V_e(\mathbf{S})$ seems to be independent of μ, whereas in the connected regime ($p > p_c$), $V_e(\mathbf{S})$ decreases significantly as μ increases. The natural fracture system has a connectivity state close to the percolation threshold ($p \approx p_c$) and its $V_e(\mathbf{S})$ is generally fit to the trend predicted from the synthetic fracture networks. The large variation of $V_e(\mathbf{S})$ for the natural fracture networks is related to their anisotropic nature, such that fracture deformation and interaction are strongly affected by the orientation of tectonic stresses relative to the orientation of fracture sets.

4. Discussion and Conclusions

The connectivity of fracture networks has been found having important influences on the mechanical and hydrological behavior of fractured formations (Davy et al., 2010; de Dreuzy et al., 2001a, 2001b; Harthong et al., 2012). In this work, we further elucidate its impact on stress distribution in geological media. Significant stress variability emerges if the fracture system is well connected and subjected to a critically stressed state; for example, the tectonic stress ratio is close to the theoretical value of 3.1 given that the friction coefficient equals to 0.6 (Zoback, 2007). The results also suggest that stress variability is more dominated by matrix resistance if fractures are disconnected, but more dependent on frictional sliding of fractures if the system is well connected. The observed dependency of stress perturbation on the geometry of fracture systems is potentially related to the reported fractal phenomenon of stress distributions in the field (Day-Lewis et al., 2010; Shamir & Zoback, 1992). The fractal geometry of fracture networks that lacks a representative elementary volume may lead to complex scale effects of stress variability, especially when the system is under a critically stressed state.

It is worth emphasizing that we propose a novel tensor-based framework, which processes stress data in an integrated form and does not violates their inherent tensorial nature (Gao & Harrison, 2016, 2018), for

characterizing stress variability in fractured rocks. This formalism aims to improve the conventional decoupled analysis, which customarily separates the information of stress magnitude/orientation and may lead to biased interpretations as also has been recognized by Hudson and Cooling (1988).

To conclude, we quantitatively investigated the underlying correlation between fracture network properties and stress variability in geological media. The stress fields under different tectonic stress conditions were determined from numerical simulations and further analyzed using a novel mathematical approach that fully honors their tensorial nature. The local stress perturbation, quantified using the Euclidean distance of a local stress tensor to the mean stress tensor, exhibited a positive, linear correlation with the local fracture intensity, measured as the total fracture length per unit area within a local sampling window. The overall stress dispersion was characterized using the effective variance of the entire stress tensor field. We found that the connectivity of fracture networks plays a critical role in controlling the strain/stress distribution in geological media. Significant strain localization and stress dispersion occur in a well-connected fracture system under a critically stressed state for frictional sliding. The results of this paper have important implications for estimating the stress state in the Earth's crust based on geometric/strain measurements of fracture populations for earthquake predictions and geo-engineering designs.

Acknowledgments
We thank the two anonymous reviewers and the Editor Andrew V. Newman for their very constructive comments that significantly improved the manuscript. All the data of numerical simulation results in this paper are publicly available at http://doi.org/10.5281/zenodo.1172190.

References

Ackermann, R. V., & Schlische, R. W. (1997). Anticlustering of small normal faults around larger faults. *Geology*, *25*(12), 1127–1130. https://doi.org/10.1130/0091-7613(1997)025<1127:AOSNFA>2.3.CO;2

Amadei, B., & Stephansson, O. (1997). *Rock Stress and its Measurement*. London: Springer. https://doi.org/10.1007/978-94-011-5346-1

Barton, C. A., & Zoback, M. D. (1994). Stress perturbations associated with active faults penetrated by boreholes: Possible evidence for near-complete stress drop and a new technique for stress magnitude measurement. *Journal of Geophysical Research*, *99*(B5), 9373–9390. https://doi.org/10.1029/93JB03359

Bell, J. S., & Gough, D. I. (1979). Northeast-southwest compressive stress in Alberta evidence from oil wells. *Earth and Planetary Science Letters*, *45*(2), 475–482. https://doi.org/10.1016/0012-821X(79)90146-8

Bonnet, E., Bour, O., Odling, N. E., Davy, P., Main, I., Cowie, P., & Berkowitz, B. (2001). Scaling of fracture systems in geological media. *Reviews of Geophysics*, *39*(3), 347–383. https://doi.org/10.1029/1999RG000074

Bour, O., & Davy, P. (1997). Connectivity of random fault networks following a power law fault length distribution. *Water Resources Research*, *33*(7), 1567–1583. https://doi.org/10.1029/96WR00433

Bour, O., & Davy, P. (1999). Clustering and size distributions of fault patterns: Theory and measurements. *Geophysical Research Letters*, *26*(13), 2001–2004. https://doi.org/10.1029/1999GL900419

Bour, O., Davy, P., Darcel, C., & Odling, N. E. (2002). A statistical scaling model for fracture network geometry, with validation on a multiscale mapping of a joint network (Hornelen Basin, Norway). *Journal of Geophysical Research*, *107*(B6), 2113. https://doi.org/10.1029/2001JB000176

Bruno, M. S., & Winterstein, D. F. (1992). *Some influences of stratigraphy and structure on reservoir stress orientation*. Paper presented at 67th Annual Technical Conference and Exhibition of the Society of Petroleum Engineers, Washington, DC. https://doi.org/doi.org/10.2118/24746-MS

Byerlee, J. (1978). Friction of rocks. *Pure and Applied Geophysics*, *116*(4–5), 615–626. https://doi.org/10.1007/BF00876528

Darcel, C., Bour, O., & Davy, P. (2003). Cross-correlation between length and position in real fracture networks. *Geophysical Research Letters*, *30*(12), 1650. https://doi.org/10.1029/2003GL017174

Darcel, C., Bour, O., Davy, P., & de Dreuzy, J.-R. (2003). Connectivity properties of two-dimensional fracture networks with stochastic fractal correlation. *Water Resources Research*, *39*(10), 1272. https://doi.org/10.1029/2002WR001628

Davy, P., Le Goc, R., Darcel, C., Bour, O., de Dreuzy, J.-R., & Munier, R. (2010). A likely universal model of fracture scaling and its consequence for crustal hydromechanics. *Journal of Geophysical Research*, *115*, B10411. https://doi.org/10.1029/2009JB007043

Day-Lewis, A., Zoback, M., & Hickman, S. (2010). Scale-invariant stress orientations and seismicity rates near the San Andreas Fault. *Geophysical Research Letters*, *37*, L24304. https://doi.org/10.1029/2010GL045025

Dershowitz, W. S., & Herda, H. H. (1992). *Interpretation of fracture spacing and intensity*. Paper presented at 33th U.S. Symposium on Rock Mechanics, Santa Fe, USA.

de Dreuzy, J.-R., Davy, P., & Bour, O. (2001a). Hydraulic properties of two-dimensional random fracture networks following a power law length distribution: 1. Effective connectivity. *Water Resources Research*, *37*(8), 2065–2078. https://doi.org/10.1029/2001WR900011

de Dreuzy, J.-R., Davy, P., & Bour, O. (2001b). Hydraulic properties of two-dimensional random fracture networks following a power law length distribution: 2. Permeability of networks based on lognormal distribution of apertures. *Water Resources Research*, *37*(8), 2079–2095. https://doi.org/10.1029/2001WR900010

Gao, K. (2017). Contribution to tensor-based stress variability characterisation in rock mechanics, (Doctoral dissertation). Toronto, ON: University of Toronto. https://tspace.library.utoronto.ca/handle/1807/78996

Gao, K., & Harrison, J. P. (2016). Mean and dispersion of stress tensors using Euclidean and Riemannian approaches. *International Journal of Rock Mechanics and Mining Sciences*, *85*, 165–173. https://doi.org/10.1016/j.ijrmms.2016.03.019

Gao, K., & Harrison, J. P. (2017). Generation of random stress tensors. *International Journal of Rock Mechanics and Mining Sciences*, *94*, 18–26. https://doi.org/10.1016/j.ijrmms.2016.12.011

Gao, K., & Harrison, J. P. (2018). Multivariate distribution model for stress variability characterisation. *International Journal of Rock Mechanics and Mining Sciences*, *102*, 144–154. https://doi.org/10.1016/j.ijrmms.2018.01.004

Gao, K., Harrison, J. P., Lei, Q., & Latham, J.-P. (2017). Investigating the relationship between far-field stress and local values of the stress tensor. *Procedia Engineering*, *191*, 536–542. https://doi.org/10.1016/j.proeng.2017.05.215

Gentle, J. E. (2007). *Matrix algebra: Theory, computations, and applications in statistics*. New York: Springer. https://doi.org/10.1007/978-0-387-70873-7

Haimson, B. C. (1975). The state of stress in the Earth's crust. *Reviews of Geophysics*, *13*(3), 350–352. https://doi.org/10.1029/RG013i003p00350

Harthong, B., Scholtès, L., & Donzé, F. V. (2012). Strength characterization of rock masses, using a coupled DEM-DFN model. *Geophysical Journal International*, *191*(2), 467–480. https://doi.org/10.1111/j.1365-246X.2012.05642.x

Hast, N. (1969). The state of stress in the upper part of the Earth's crust. *Tectonophysics*, *8*(3), 169–211. https://doi.org/10.1016/0040-1951(69)90097-3

Hickman, S., & Zoback, M. (2004). Stress orientations and magnitudes in the SAFOD pilot hole. *Geophysical Research Letters*, *31*, L15S12. https://doi.org/10.1029/2004GL020043

Hudson, J. A., & Cooling, C. M. (1988). In situ rock stresses and their measurement in the U.K.—Part I. The current state of knowledge. *International Journal of Rock Mechanics and Mining Science and Geomechanics Abstracts*, *25*(6), 363–370. https://doi.org/10.1016/0148-9062(88)90976-X

Kropotkin, P. N. (1972). The state of stress in the Earth's crust as based on measurements in mines and on geophysical data. *Physics of the Earth and Planetary Interiors*, *6*(4), 214–218. https://doi.org/10.1016/0031-9201(72)90002-7

Lama, R. D., & Vutukuri, V. S. (1978). *Handbook on mechanical properties of rocks: Testing techniques and results* (Vol. 2). Clausthal: Trans. Tech. Publications.

Lei, Q., Latham, J.-P., & Tsang, C.-F. (2017). The use of discrete fracture networks for modelling coupled geomechanical and hydrological behaviour of fractured rocks. *Computers and Geotechnics*, *85*, 151–176. https://doi.org/10.1016/j.compgeo.2016.12.024

Lei, Q., Latham, J.-P., Tsang, C.-F., Xiang, J., & Lang, P. (2015). A new approach to upscaling fracture network models while preserving geostatistical and geomechanical characteristics. *Journal of Geophysical Research: Solid Earth*, *120*, 4784–4807. https://doi.org/10.1002/2014JB011736

Lei, Q., & Wang, X. (2016). Tectonic interpretation of the connectivity of a multiscale fracture system in limestone. *Geophysical Research Letters*, *43*, 1551–1558. https://doi.org/10.1002/2015GL067277

Lin, W., Yeh, E. C., Hung, J. H., Haimson, B., & Hirono, T. (2010). Localized rotation of principal stress around faults and fractures determined from borehole breakouts in hole B of the Taiwan Chelungpu-fault Drilling Project (TCDP). *Tectonophysics*, *482*(1–4), 82–91. https://doi.org/10.1016/j.tecto.2009.06.020

Lin, W., Yeh, E. C., Ito, H., Hung, J. H., Hirono, T., Soh, W., et al. (2007). Current stress state and principal stress rotations in the vicinity of the Chelungpu fault induced by the 1999 Chi-Chi, Taiwan, earthquake. *Geophysical Research Letters*, *34*, L16307. https://doi.org/10.1029/2007GL030515

Marrett, R., & Allmendinger, R. W. (1991). Estimates of strain due to brittle faulting: Sampling of fault populations. *Journal of Structural Geology*, *13*(6), 735–738. https://doi.org/10.1016/0191-8141(91)90034-G

Martin, C. D., & Chandler, N. A. (1993). Stress heterogeneity and geological structures. *International Journal of Rock Mechanics and Mining Science and Geomechanics Abstracts*, *30*(7), 993–999. https://doi.org/10.1016/0148-9062(93)90059-M

Mauldon, M., Dunne, W. M., & Rohrbaugh, M. B. (2001). Circular scanlines and circular windows: New tools for characterizing the geometry of fracture traces. *Journal of Structural Geology*, *23*(2–3), 247–258. https://doi.org/10.1016/S0191-8141(00)00094-8

McGarr, A., & Gay, N. C. (1978). State of stress in the Earth's crust. *Annual Review of Earth and Planetary Sciences*, *6*(1), 405–436. https://doi.org/10.1146/annurev.ea.06.050178.002201

Mcnamara, D. D., Massiot, C., Lewis, B., & Wallis, I. C. (2015). Heterogeneity of structure and stress in the Rotokawa Geothermal Field, New Zealand. *Journal of Geophysical Research: Solid Earth*, *120*, 1243–1262. https://doi.org/10.1002/2014JB011480

Munjiza, A. (2004). *The Combined Finite-Discrete Element Method*. London: Wiley. https://doi.org/10.1002/0470020180

Odling, N. E. (1997). Scaling and connectivity of joint systems in sandstones from western Norway. *Journal of Structural Geology*, *19*(10), 1257–1271. https://doi.org/10.1016/S0191-8141(97)00041-2

Peña, D., & Rodríguez, J. (2003). Descriptive measures of multivariate scatter and linear dependence. *Journal of Multivariate Analysis*, *85*(2), 361–374. https://doi.org/10.1016/S0047-259X(02)00061-1

Pennec, X. (2009). Statistical computing on manifolds: From Riemannian geometry to computational anatomy. In N. Frank (Ed.), *Emerging Trends in Visual Computing* (pp. 347–386). Berlin: Springer. https://doi.org/10.1007/978-3-642-00826-9_16

Pollard, D. D., & Segall, P. (1987). Theoretical displacements and stresses near fractures in rock: With applications to faults, joints, veins, dikes, and solution surfaces. In B. K. Atkinson (Ed.), *Fracture Mechanics of Rock* (pp. 277–349). San Diego: Academic Press. https://doi.org/10.1016/B978-0-12-066266-1.50013-2

Rajabi, M., Tingay, M., King, R., & Heidbach, O. (2017). Present-day stress orientation in the Clarence-Moreton Basin of New South Wales, Australia: A new high density dataset reveals local stress rotations. *Basin Research*, *29*, 622–640. https://doi.org/10.1111/bre.12175

Robinson, P. C. (1983). Connectivity of fractures systems—A percolation theory approach. *Journal of Physics A: Mathematical and General*, *16*(3), 605–614. https://doi.org/10.1088/0305-4470/16/3/020

Robinson, P. C. (1984). Numerical calculations of critical densities for lines and planes. *Journal of Physics A: Mathematical and General*, *17*(14), 2823–2830. https://doi.org/10.1088/0305-4470/17/14/025

Sahara, D. P., Schoenball, M., Kohl, T., & Müller, B. I. R. (2014). Impact of fracture networks on borehole breakout heterogeneities in crystalline rock. *International Journal of Rock Mechanics and Mining Sciences*, *71*, 301–309. https://doi.org/10.1016/j.ijrmms.2014.07.001

Schoenball, M., & Davatzes, N. C. (2017). Quantifying the heterogeneity of the tectonic stress field using borehole data. *Journal of Geophysical Research: Solid Earth*, *122*, 6737–6756. https://doi.org/10.1002/2017JB014370

Segall, P., & Pollard, D. D. (1983). Joint formation in granitic rock of the Sierra Nevada. *Geological Society of America Bulletin*, *94*(5), 563–575. https://doi.org/10.1130/0016-7606(1983)94<563:JFIGRO>2.0.CO;2

Shamir, G., & Zoback, M. D. (1992). Stress orientation profile to 3.5 km depth near the San Andreas Fault at Cajon Pass, California. *Journal of Geophysical Research*, *97*(B4), 5059–5080. https://doi.org/10.1029/91JB02959

Stephansson, O., Ljunggren, C., & Jing, L. (1991). Stress measurements and tectonic implications for Fennoscandia. *Tectonophysics*, *189*(1-4), 317–322. https://doi.org/10.1016/0040-1951(91)90504-L

Townend, J., & Zoback, M. D. (2004). Regional tectonic stress near the San Andreas fault in central and southern California. *Geophysical Research Letters*, *31*, L15S11. https://doi.org/10.1029/2003GL018918

Valley, B. C. (2007). The relation between natural fracturing and stress heterogeneities in deep-seated crystalline rocks at Soultz-sous- Forêts (France), (Doctoral Dissertation). Zurich: Swiss Federal Institute of Technology Zurich.

Yale, D. P. (2003). Fault and stress magnitude controls on variations in the orientation of in situ stress. In M. Ameen (Ed.), *Fracture and In-Situ Stress Characterization of Hydrocarbon Reservoirs. Geological Society of London, Special Publications*, 209, 55–64. https://doi.org/10.1144/GSL.SP.2003.209.01.06

Zoback, M. D. (2007). *Reservoir geomechanics*. Cambridge, UK: Cambridge University Press. https://doi.org/10.1017/CBO9780511586477

Zoback, M. L. (1992). First- and second-order patterns of stress in the lithosphere: The world stress map project. *Journal of Geophysical Research*, *97*(B8), 11,703–11,728. https://doi.org/10.1029/92JB00132

Zoback, M. L., Zoback, M. D., Adams, J., Assumpção, M., Bell, S., Bergman, E. A., et al. (1989). Global patterns of tectonic stress. *Nature*, *341*(6240), 291–298. https://doi.org/10.1038/341291a0